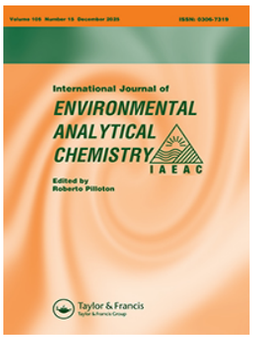

International Journal of Environmental Analytical Chemistry

ISSN: 0306-7319 (Print) 1029-0397 (Online) Journal homepage: www.tandfonline.com/journals/geac20

Integrated biomass algae @ cross-linked pyromellitic dianhydride chitosan biocomposite for methyl violet 2B adsorption: modelling and experiment design optimization

Hasan M. Agha, Muna Abd Ul Rasool Al-Kazragi, Ali H. Jawad, Lee D. Wilson, Hussein A. Kazem & Zeid A. ALOthman

To cite this article: Hasan M. Agha, Muna Abd Ul Rasool Al-Kazragi, Ali H. Jawad, Lee D. Wilson, Hussein A. Kazem & Zeid A. ALOthman (30 Oct 2025): Integrated biomass algae @ cross-linked pyromellitic dianhydride chitosan biocomposite for methyl violet 2B adsorption: modelling and experiment design optimization, International Journal of Environmental Analytical Chemistry, DOI: 10.1080/03067319.2025.2576558

To link to this article: https://doi.org/10.1080/03067319.2025.2576558

INTERNATIONAL JOURNAL OF ENVIRONMENTAL ANALYTICAL CHEMISTRY
https://doi.org/10.1080/03067319.2025.2576558

Integrated biomass algae @ cross-linked pyromellitic dianhydride chitosan biocomposite for methyl violet 2B adsorption: modelling and experiment design optimization

Hasan M. Agha[a,b], Muna Abd Ul Rasool Al-Kazragi[c], Ali H. Jawad[a,b,d], Lee D. Wilson[e], Hussein A. Kazem[f] and Zeid A. ALOthman[g]

[a]Faculty of Applied Sciences, Universiti Teknologi MARA, Shah Alam, Malaysia; [b]Advanced Biomaterials and Carbon Development (ABCD) Research Group, Faculty of Applied Sciences, Universiti Teknologi MARA, Shah Alam, Malaysia; [c]Department of Chemistry, University of Baghdad, College of Education for Pure Science Ibn-Al-Haitham, Baghdad, Iraq; [d]Environmental and Atmospheric Sciences Research Group, Scientific Research Center, Al-Ayen University, Nasiriyah, Iraq; [e]Department of Chemistry, University of Saskatchewan, Saskatoon, SK, Canada; [f]Electrical and computer engineering, Faculty of Engineering-Sohar University, Sohar, Oman; [g]Advanced Materials Research Chair, Chemistry Department, College of Science, King Saud University, Riyadh, Saudi Arabia

ABSTRACT

A new adsorbent was developed by integrating algae biomass (AG) into a chitosan (CN) matrix, followed by structural enhancement via crosslinking with pyromellitic dianhydride (PMDA) through a hydrothermal synthesis approach. This process resulted in the formation of a robust AG@CN-PMDA composite with improved physicochemical characteristics suitable for advanced adsorption applications. The AG@CN-PMDA composite was evaluated for its efficiency in removal of the cationic dye methyl violet 2B (MV 2B) from aqueous solution. The adsorption process was refined through the Box-Behnken design (RSM-BBD), evaluating three essential parameters: adsorbent dosage (A: 0.02–0.1 g/100 mL), pH (B: 4–10), and time (C: 5–20 min). The ideal conditions for attaining the best removal rate for MV 2B (86%) were determined based on the desirability function optimisation results, corresponding to 0.09 g/100 mL of AG@CN-PMDA, at a pH of 6.9 and time of 9.45 min. The adsorption isothermal analysis revealed a close fit between the experimental data of MV 2B adsorption and both the Temkin and Langmuir models, with the Temkin model showing a slightly better correlation. Furthermore, the adsorption kinetics are well-described by the pseudo-second-order model. The maximum adsorption capacity of AG@CN-PMDA was 162.3 mg/g at 25°C. The adsorption of MV 2B onto AG@CN-PMDA was spontaneous, endothermic, and entropy-driven as evidenced by negative ΔG° values. The binding of MV 2B dye onto the AG@CN-PMDA composite was facilitated through mechanisms such as hydrogen bonding, π–π stacking, and electrostatic attraction. These findings demonstrate that AG@CN-PMDA is an effective and sustainable adsorbent for the removal of cationic dyes from industrial effluents.

ARTICLE HISTORY
Received 27 August 2025
Accepted 13 October 2025

KEYWORDS
Adsorption; algae; Box-Behnken design; chitosan; crosslinking; pyromellitic dianhydride

CONTACT Ali H. Jawad ali288@uitm.edu.my; ahjm72@gmail.com
Supplemental data for this article can be accessed online at https://doi.org/10.1080/03067319.2025.2576558

1. Introduction

Water contamination is a pressing global issue mainly driven by rapid industrialisation and urbanisation [1,2]. Many industries discharge untreated effluents directly into natural water bodies, which intensify pollution levels [3,4]. The textile, food, cosmetics, and paper industries are among the largest contributors due to their extensive use of synthetic dyes, which generate vast volumes of toxic wastewater [5,6]. Cationic dyes such as methylene blue, methyl violet, and crystal violet are highly soluble, persistent, and hazardous. They hinder photosynthesis in aquatic systems, disrupt ecological balance, and pose severe health risks including nausea, carcinogenicity, tachycardia, and genetic damage [7,8]. Methyl violet 2B (MV 2B), a triphenylmethane dye, is particularly mutagenic and toxic, capable of disturbing cellular functions and accumulating in living organisms, thus threatening biodiversity and long-term ecosystem stability [9,10]. These concerns emphasise the urgent need for efficient and sustainable dye removal methods.

Consequently, the advancement of innovative technology capable of efficiently eliminating these pollutants from industrial waste prior to their discharge into aquatic environments has become a paramount issue. Researchers have investigated and used several sophisticated methods for the remediation of dye-contaminated wastewater, including adsorption [11], activated sludge process [12], photocatalysis [13], coagulation [14], ion exchange [15], nanofiltration [16], and osmosis [17]. Adsorption has emerged as a highly efficient and effective method, providing features like cost-effectiveness, user-friendliness, environmental sustainability, minimum waste generation, and elevated removal efficiency [18,19].

Chitosan (CN) is employed in a variety of fields, such as biotechnology, pharmaceuticals, wastewater treatment, and biomedicine, due to its mucoadhesive properties, adsorption capacities, and biodegradability, as well as its natural prevalence and non-toxic nature [20,21]. The existence of reactive amino and hydroxyl groups in CN has garnered considerable attention for wastewater remediation applications, chiefly owing to its exceptional reactivity and advantageous physicochemical characteristics [22]. Nevertheless, CN is afflicted by numerous deficiencies, including insufficient mechanical strength, rapid agglomeration, and solubility in low-concentration acids [23]. Therefore, enhancing the physicochemical properties of CN, including its adsorption effectiveness, chemical durability, and surface area, is essential. To mitigate these constraints, synthetic modification tactics has been employed that includes covalent cross-linking [24], grafting [25], and integration with biomaterials [26].

The covalent cross-linking procedure of CN utilises its binding sites to interact with different chemical cross-linking agents, leading to the creation of covalent bonds [27]. The covalent links are subsequently arranged to construct a cross-linked CN with a defined network architecture [28]. Cross-linking of chitosan yields enhanced mechanical integrity, improved resistance to acidic degradation, and superior dimensional stability, owing to the formation of covalent linkages that reinforce the biopolymer network structure [29]. Pyromellitic dianhydride (PMDA) is an environmentally benign crosslinker agent characterised by many – COOH groups that readily react with – NH_2 on CN. Numerous investigations have shown that PMDA-modified adsorbents display effective adsorption properties [30]. Cross-linked CN composites are extensively used for removal of synthetic dyes in contaminated aquatic environments [31,32].

To enhance the adsorption capability of CN-based composites, several intriguing inorganic and biomaterials, including lignin [33], algae [34], TiO_2 [35], and gum [36], have been used as additives to yield improved adsorption properties. The integration of inorganic/biomaterials seeks to use its distinctive properties and functions to improve the adsorptive capacity of CN-based composites. Adding algae (AG) to CN-based compounds might make them more resistant to chemicals, more effective at adsorbing, and structural enhancement [37]. The latest research has shown the remarkable adsorption capacity of AG in removing diverse contaminants, such as heavy metals [38], pharmaceuticals [39], and organic dyes [40], from polluted water. Environmental remediation and the promotion of sustainability are two areas that may benefit greatly from the innovative and long-term solutions offered by AG-based biomaterials [41].

Therefore, the aim of this study is to fabricate a sustainable composite adsorbent, designated as AG@CN-PMDA by incorporating AG into the polymeric matrix of CN, followed by covalent crosslinking with PMDA. The adsorption efficacy of AG@CN-PMDA was assessed for the removal of MV 2B dye from aqueous media. The response surface methodology-Box-Behnken design (RSM-BBD) was utilised to systematically improve the principal operational elements affecting the adsorption process. The parameters were evaluated that affect the adsorption process and include the AG@CN-PMDA dose, duration, and pH. An analysis of the adsorption capacity and efficacy of AG@CN-PMDA for the removal of MV 2B may provide a full knowledge of these factors.

2. Materials and methods

2.1. Materials

PMDA ($C_{10}H_2O_6$, molecular weight: 218.12 g/mol) was provided by Shanghai Aladdin Biochemical Technology Co., Ltd., China. Medium molecular weight CN powder with a 75% deacetylation degree was obtained from Sigma-Aldrich. AG was obtained from Henan Yuzhong Bioengineering, China. MV 2B, $C_{24}H_{28}ClN_3$, molecular weight: 393.94 g/mol, wavelength: 575 nm) was procured from Tianjin Kemiou Chemical Reagent, China, and utilised as the standard cationic dye for adsorption tests. Supplementary reagents, comprising sodium hydroxide (NaOH), acetic acid (CH_3COOH), sodium chloride (NaCl), and hydrochloric acid (HCl), were procured from R&M Chemicals and utilised without additional purification.

2.2. Synthesis of hydrothermally cross-linked AG@CN-PMDA

The synthesis of the AG@CN-PMDA composite was performed according to the following procedure. Initially, 1 g of CN flakes and 1 g of AG powder were mixed in a 1:1 ratio, as described in previous work [42], where 75 mL of 5% acetic acid was added gradually. The mixture was magnetically stirred at room temperature for 24 h to completely dissolve the CN flakes and facilitate homogeneous interaction with AG. The resulting mixture was then subjected to ultrasonic treatment at a frequency of 40 kHz and a power output of 20 W for 25 min to enhance homogeneity. The viscous suspension obtained was subsequently added dropwise into a 0.5 M NaOH solution by syringe, resulting in the formation of bead-like AG@CN structures. These beads were repeatedly washed with distilled water until a neutral pH was achieved. For the crosslinking step, 10 mL of 2% PMDA solution was

prepared, and the reaction was conducted in a hydrothermal reactor containing 2 g of AG@CN beads at 100°C for 4 h. After this procedure, the synthesised beads were subjected to extensive washing with distilled water. The AG@CN-PMDA beads were then dried inside the oven for 24 h at 60°C. To achieve consistency in particle size for adsorption tests, the AG@CN-PMDA sample was ground by using a mortar and pestle to provide particles measuring 250 µm. Figure 1 delineates the steps for the preparation of AG@CN-PMDA. Refer to the supplementary data (Text S1) for additional details on the characterisation of AG@CN-PMDA composite, including the techniques employed.

2.3. Statistical optimisation methodology

RSM is acknowledged as a potent statistical instrument for optimising adsorption processes by improving removal efficiency and reducing the necessity for undue

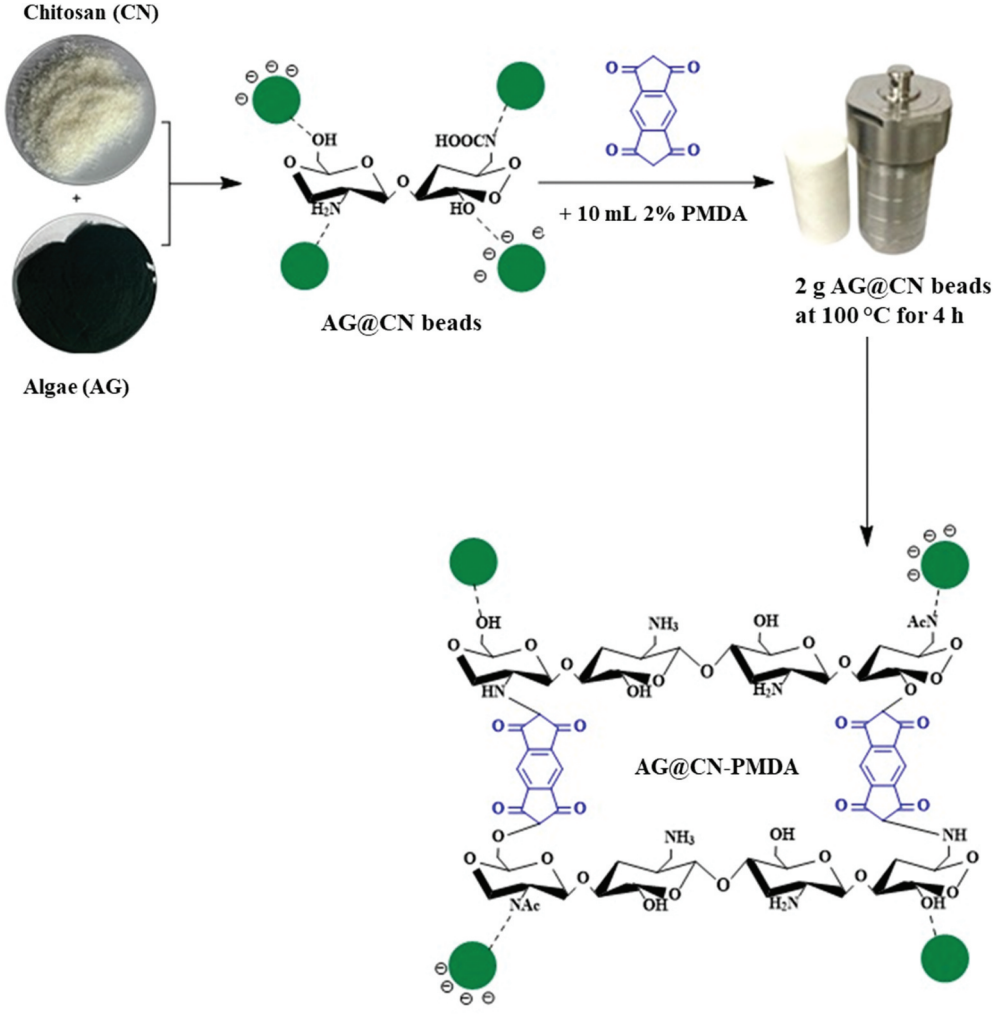

Figure 1. Synthesis strides of AG@CN-PMDA.

experimental trials [43]. RSM-BBD was applied to systematically examine the influence of three key parameters AG@CN-PMDA dose, contact time, and solution pH on the removal efficiency of MV 2B dye. Experimental design and optimisation were carried out using Design-Expert software (version 13.0, Stat-Ease Inc., Minneapolis, USA), ensuring statistical reliability and accuracy in the analysis of the obtained data. Consequently, preliminary tests were conducted to ascertain the functional rates of the adsorption critical factors for the removal of MV 2B by the AG@CN-PMDA composite, as indicated in Table 1. By applying a regression model to the experimental data, the correlation between the output (MV 2B removal) and the input variables may be estimated. Equation (1) illustrates this relationship:

$$Y = \beta_0 + \sum \beta_i X_i + \sum \beta_{ii} X_i^2 + \sum \sum \beta_{ij} X_i X_j \quad (1)$$

Y refers to the response parameter, β_0 constant coefficient, β_i, β_{ij}, and β_{ii} coefficients for the linear, interaction, and quadratic expressions, respectively, and X_i and X_j are the parameter values. Analysing the regression model enables the estimation of ideal operating parameters for obtaining the target MV 2B elimination during the adsorption process. The BBD tests for the removal of MV 2B using the AG@CN-PMDA are included in Table 2. In each experimental trial, 100 mL of MV 2B dye solution was produced, to which a specified quantity of adsorbent was introduced in a 250 mL conical flask. The mixture was stirred with an orbital shaker at 100 rpm for a designated period. Following the adsorption procedure, the adsorbent was isolated from the solution with a 0.45 µm syringe filter. The residual dye content in the filtrate was quantified using a UV – Vis spectrophotometer

Table 1. Codes and actual variables and their levels in BBD.

Codes	Variables	Level 1 (−1)	Level 2 (0)	Level 3 (+1)
A	AG@CN-PMDA dose (g/100 mL)	0.02	0.06	0.1
B	Time (min)	2	11	20
C	pH	4	7	10

Table 2. Experimental matrix based on BBD approach for designing experiments and the corresponding response (MV 2B removal).

Run	A: AG@CN-PMDA dose (g/100 mL)	B: Time (min)	C: pH	MV 2B removal (%)
1	0.02	2	7	42.2
2	0.1	2	7	78.9
3	0.02	20	7	52.9
4	0.1	20	7	82.8
5	0.02	11	4	47.8
6	0.1	11	4	79.8
7	0.02	11	10	43.2
8	0.1	11	10	85.8
9	0.06	2	4	52.8
10	0.06	20	4	69.8
11	0.06	2	10	62.9
12	0.06	20	10	64.3
13	0.06	11	7	71.3
14	0.06	11	7	74.1
15	0.06	11	7	73.3
16	0.06	11	7	75.2
17	0.06	11	7	77.1

(HACH DR 3900) at a peak wavelength (λ_{max}) of 575 nm. The efficiency of dye removal was determined using Equation (2):

$$R\ \% = \frac{(C_o - C_e)}{C_o} \times 100 \tag{2}$$

Where C_o and C_e denote the initial and equilibrium concentrations (mg/L) of dye, before and after adsorption, respectively.

2.4. Adsorption study

A desirability function tool was employed to ascertain the ideal values for the adsorption variables. The desirability function (cf. Figure 2) for MV 2b removal (%) by AG@CN-PMDA demonstrated that the ideal parameters for maximal MV 2B removal (86%) included an AG@CN-PMDA (dose = 0.09 g/100 mL, pH = 6.9, and a period of 9.5 min). The optimal conditions obtained from the BBD model were initially verified through survey experiments, conducted in triplicate to ensure reliability. The results demonstrated removal efficiency closely matching the predicted value from the desirability function (85.9%), thereby confirming the model's accuracy. These optimised parameters were subsequently applied in batch equilibrium studies using varying initial concentrations of MV 2B dye ranging from 20 to 150 mg/L. All experiments were conducted in accordance with the procedure detailed in Section 2.3. The adsorption capacity of the adsorbent (q_e, mg/g) was calculated using Equation (3):

$$q_e = \frac{(C_o - C_e)V}{m} \tag{3}$$

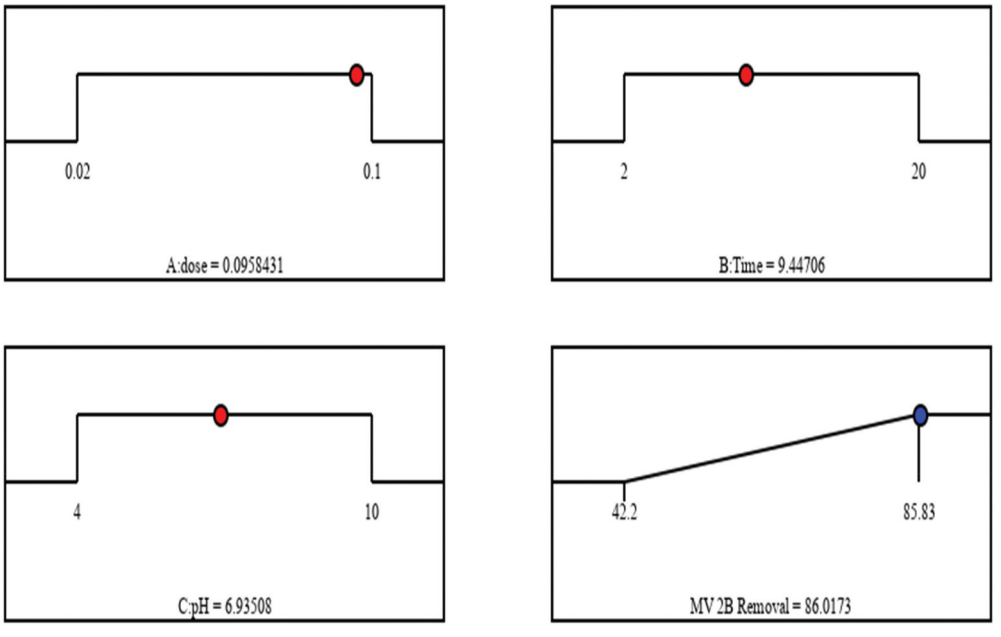

Figure 2. Desirability function of MV 2B removal (%) by the AG@CN-PMDA composite.

The q_e (mg/g) term refers to the equilibrium adsorption capacity, V (L) indicates to the volume of MV 2B solution and m (g) refer to AG@CN-PMDA dose.

3. Results and discussion

3.1. Characterisation of AG@CN-PMDA

A Field Emission Scanning Electron Microscopy-Energy Dispersive X-ray (FESEM-EDX) analysis was performed to assess the structural characteristics and chemical components of AG@CN-PMDA before after MV 2B dye adsorption. Figure 3(a,b) display the FESEM-EDX data for the AG@CN-PMDA composite, initially and after the adsorption of MV 2B dye. Figure 3(a) illustrates that the AG@CN-PMDA surface has an uneven and coarse surface texture, marked by the presence of agglomerates and voids. After the adsorption of MV 2B, seen in Figure 3(b), the surface morphology of AG@CN-PMDA exhibits less flaws and a more refined granular texture. The decrease in surface roughness signifies the efficient adsorption of MV 2B dye onto the binding sites of AG@CN-PMDA. The EDX investigation revealed the existence of C, O, and N as the principal elements in the molecular structure of both AG@CN-PMDA composite and AG@CN-PMDA-MV 2B systems. The changes in atom content (%) observed after adsorption may suggest the binding of the MV 2B dye to

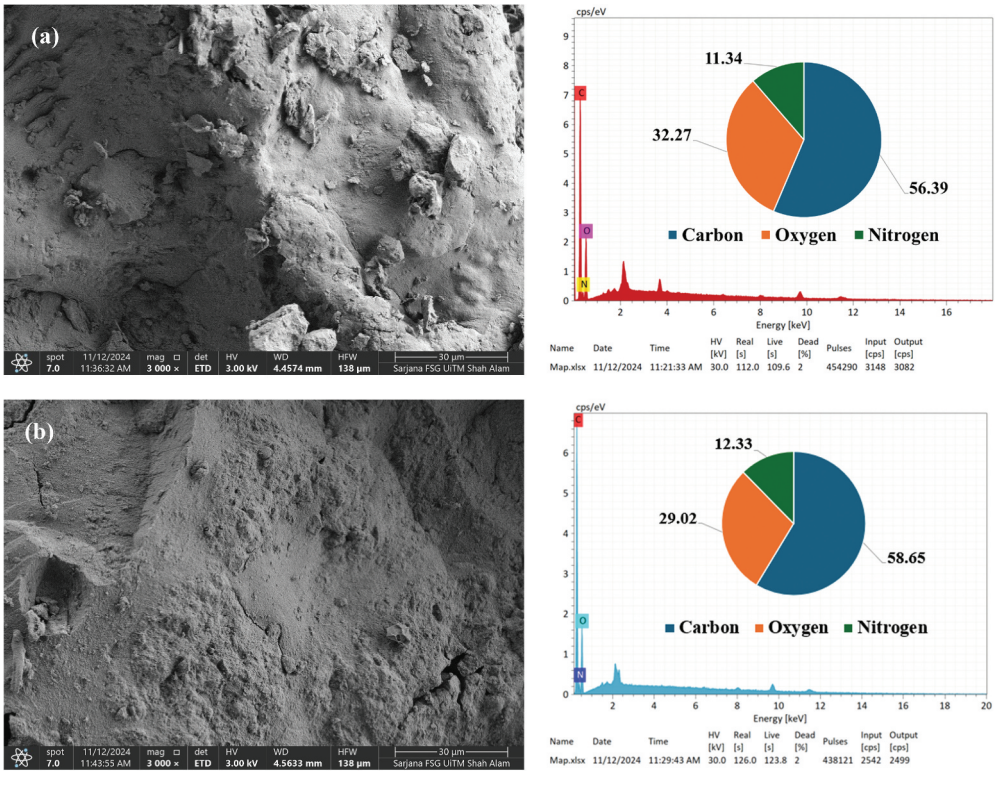

Figure 3. FESEM images and EDX results of (a) AG@CN-PMDA and (b) AG@CN-PMDA-MV 2b (after dye adsorption).

the AG@CN-PMDA surface, providing potential evidence for the adsorptive interaction between the dye and AG@CN-PMDA.

The structural characteristic of the AG@CN-PMDA composite was examined using X-ray diffraction (XRD) analysis, as depicted in Figure 4. The diffraction peaks observed at approximately $2\theta \approx 11.5°$ and 20° correspond to the semi-crystalline nature of the material, which can be attributed to the presence of hydrogen bonding between hydroxyl (–OH) and amino (-NH_2) groups within the CN chains, as well as the crystalline domains associated with the cellulose structure in AG biomass [44,45]. Additionally, a broad, low-intensity peak observed around $2\theta \approx 26.9°$ may be ascribed to residual mineral phases or partially ordered carbonaceous structures, potentially originating from the AG biomass or from structural modifications induced by PMDA incorporation [46,47]. The XRD pattern of the AG@CN-PMDA composite is consistent with previously reported profiles for pure CN, AG, and their binary composite (AG@CN, 50:50) [42], although noticeable variations are evident, particularly a reduction in peak intensity and increased broadness. These changes are indicative of successful intercalation of PMDA into the CN-AG matrix, which disrupts the ordered structure and reduces crystallinity. Such modifications in the diffraction pattern confirm the effective incorporation of PMDA into the CN-AG framework, thereby validating the formation of the AG@CN-PMDA composite.

The functional groups present in the AG@CN-PMDA composite that potentially interact with the MV 2B dye were analysed using FTIR spectroscopy prior to and after adsorption, as illustrated in Figure 5(a,b). The broad absorption band observed in the range of 3450–3300 cm^{-1} (Figure 5(a)) was attributed to the stretching vibrations

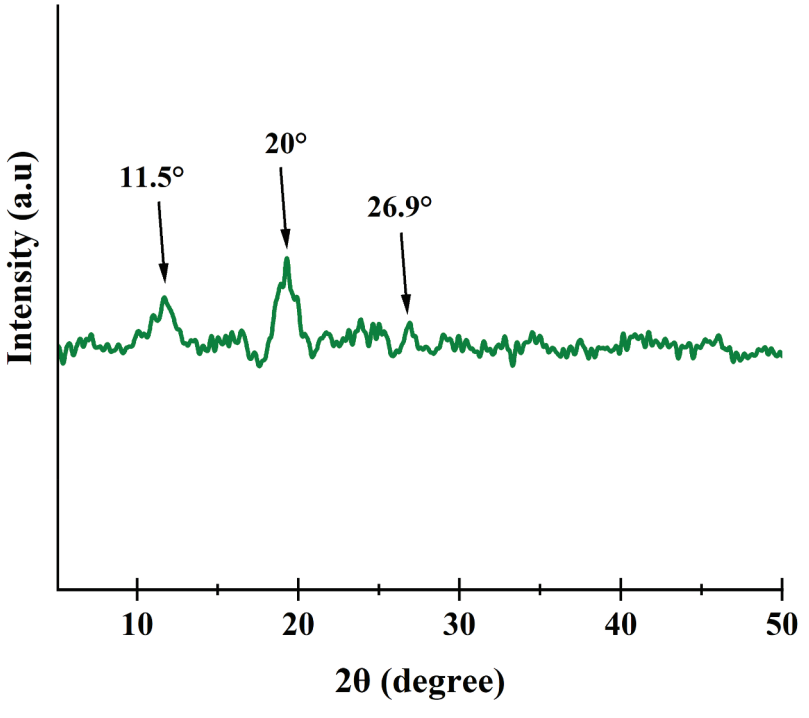

Figure 4. XRD pattern of the AG@CN-PMDA composite.

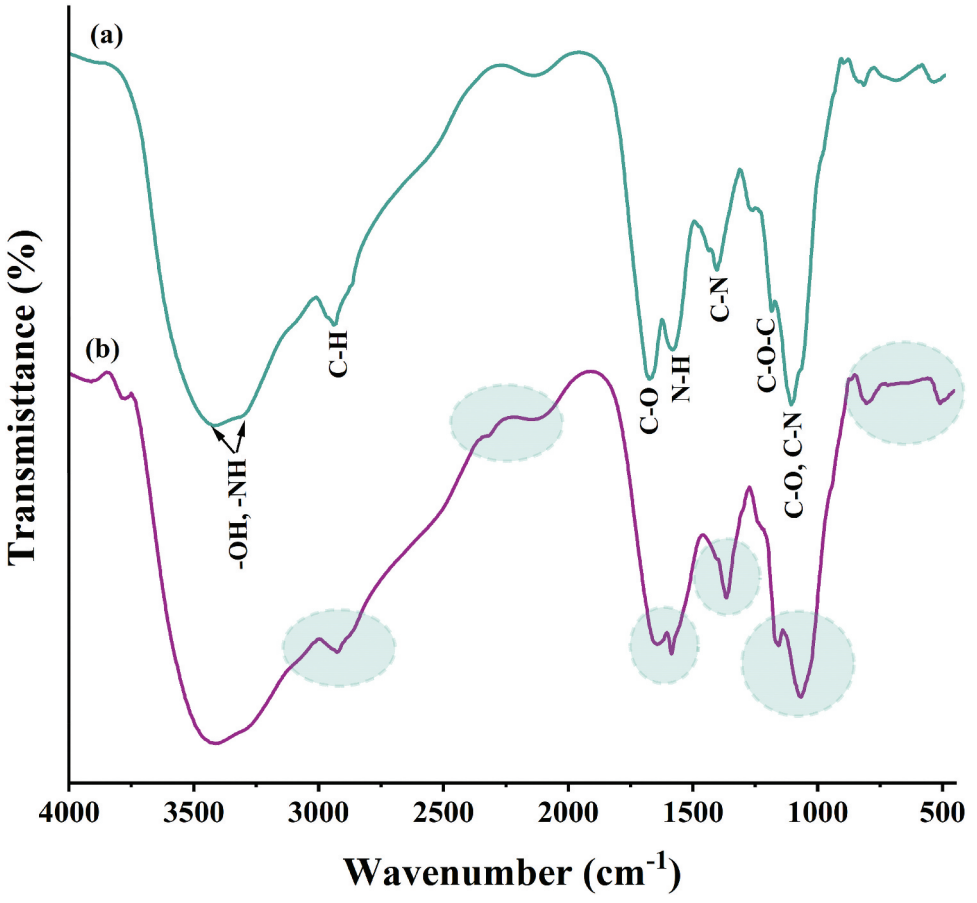

Figure 5. FTIR spectra: (a) AG@CN-PMDA and (b) AG@CN-PMDA after adsorption of the MV 2B dye.

of hydroxyl (–OH) and amine (–NH) groups, originating from AG and CN, respectively [48]. The decreased intensity of the broad peak in this region, compared to our prior findings, indicates the consumption of –OH and –NH groups due to crosslinking with PMDA [42]. This observation aligns with the chemical modifications expected during the crosslinking process, further confirming the interaction. Notable IR absorption bands detected in the AG@CN-PMDA composite have a peak at 2920 cm^{-1}, indicative of C–H stretching vibrations in $–CH_2$ and $–CH_3$ groups [49]. The band at 1650 cm^{-1} is ascribed to C=O stretching vibrations in AG, linked to functional groups like carboxylic acids (RCOOH) and ketones (RCOR), and may also suggest interactions between the amino groups of CN and the anhydride groups of PMDA, resulting in the formation of amide or imide linkages [50,51]. A band at 1550 cm^{-1}, indicative of N–H bending, further corroborates the formation of amide or imide bonds resulting from the reaction of PMDA with CN [52]. Additional bands were detected at 1380 cm^{-1} (C–N stretching), 1150 cm^{-1} (asymmetric stretching of the C–O–C bridge in CN and AG), and 1070 cm^{-1} (C–O vibration) [53–55]. Following the adsorption of MV 2B, as illustrated in Figure 5(b), the spectrum closely resembles that of AG@CN-PMDA, with noticeable alterations in several bands. This

suggests that the adsorption process of MV 2B engaged with multiple functional groups of AG@CN-PMDA.

The impact of pH on adsorption efficacy may be more accurately elucidated by identifying the point of zero charge (pH_{pzc}) of the AG@CN-PMDA. Adsorbent surfaces generally display a positive charge at pH levels below the pH_{pzc}, whereas a negative charge prevails at pH levels above the pH_{pzc} [56]. Figure 6 illustrates the pH_{pzc} curve of the AG@CN-PMDA. At pH levels above pH_{pzc}, the AG@CN-PMDA composite exhibits a negatively charged surface, facilitating the efficient adsorption of positively charged adsorbates as the MV 2B dye. When the pH surpasses the pH_{pzc} for AG@CN-PMDA (6.4), strong electrostatic interactions may develop between the negative charge of the AG@CN-PMDA composite and the positive charge of the MV 2B dye. This suggests that solutions with a pH greater than 6.4 are optimal for the adsorption of MV 2B by the AG@CN-PMDA composite.

The pH_{pzc} is conceptually comparable to the isoelectric point (IEP), as both denote the pH at which the surface bears no net charge, although they are determined by different methods. The IEP or pH_{pzc} critically influences adsorption performance by controlling surface charge interactions between the adsorbent and adsorbate. At pH values below the IEP, the positively charged surface repels cationic dye molecules such as MV 2B, whereas at pH > 6.4, the negatively charged AG@CN-PMDA surface enhances adsorption through electrostatic attraction. This observation agrees with previous studies reporting the strong dependence of cationic dye removal efficiency on surface charge behaviour and solution pH [57].

3.2. Statistical analysis

Analysis of variance (ANOVA) serves as a fundamental statistical tool for validating model significance and evaluating the robustness of the MV 2B removal model. As presented in Table 3, the ANOVA results demonstrate that the developed model exhibits a high level of

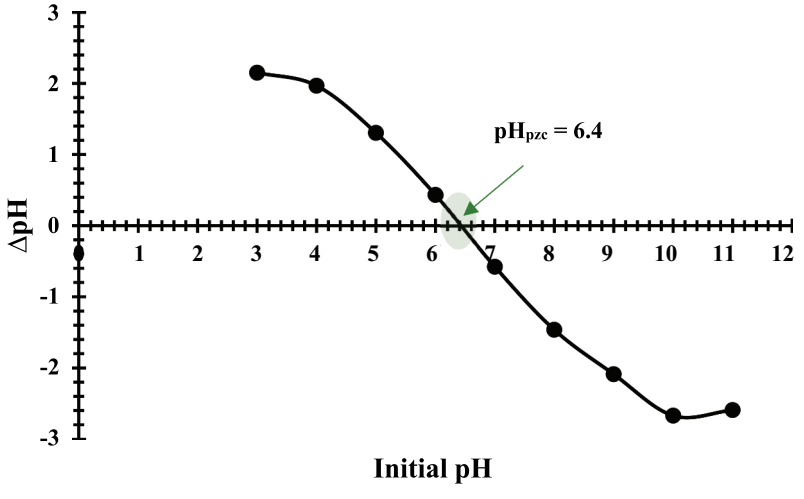

Figure 6. pH_{pzc} of the AG@CN-PMDA composite.

Table 3. Analysis of variance (ANOVA) for MV 2B removal by the AG@CN-PMDA composite.

Source	Sum of squares	df	Mean square	F-value	*p*-value	Remark
Model	3139.39	9	348.82	82.45	< 0.0001	S*
A-dose	2493.59	1	2493.59	589.39	< 0.0001	S
B-Time	136.54	1	136.54	32.27	0.0008	S
C-pH	4.52	1	4.52	1.07	0.3359	NS*
AB	11.83	1	11.83	2.80	0.1384	NS
AC	28.52	1	28.52	6.74	0.0356	S
BC	60.30	1	60.30	14.25	0.0069	S
A^2	71.15	1	71.15	16.82	0.0046	S
B^2	143.76	1	143.76	33.98	0.0006	S
C^2	147.98	1	147.98	34.98	0.0006	S
Residual	29.62	7	4.23			
Lack of Fit	10.94	3	3.65	0.7813	0.5630	NS
Pure Error	18.67	4	4.67			
Cor Total	3169.00	16				
		$R^2 = 0.9907$	Adjusted $R^2 = 0.9786$		Predicted $R^2 = 0.9355$	

Note: S*: Significant, NS*: Not Significant

statistical reliability, with an F-value of 82.45. This confirms that the model was constructed with strong confidence and predictive accuracy. Moreover, the excellent correlation between the predicted and experimental decolourisation values, supported by an R^2 value of 0.99, underscores the model's suitability and effectiveness within the BBD optimisation framework. Since the discrepancy of less than 0.2 exists between the Adjusted R^2 of 0.98 and the Predicted R^2 of 0.94, suggesting a reasonable alignment [58], as shown in Table 3. Moreover, the non-significant LOF score (0.5630) indicates that it was suitably created [59]. The effectiveness of MV 2B dye removal depends on multiple variables, excluding statistical p-values over 0.05. The MV 2B removal model produced statistically significant outcomes for the interaction and quadratic factors A, B, AC, BC, A^2, B^2, and C^2. A second-degree polynomial equation was utilised to characterise the statistical relationship between the response and the variables affecting the adsorption process. This model delineates the empirical connection between the examined components and the observed response, as seen in Equation (4).

$$MV\ 2B\ removal\ (\%) = +74.20 + 17.65A + 4.13B + 0.7512C - 1.72AB + 2.67AC - 3.88BC - 4.11A^2 - 5.84B^2 - 5.93C^2 \quad (4)$$

Graphical analysis is a crucial instrument for model validation and evaluation of residual distribution. Normal probability plots are utilised to analyse the patterns of residual distribution. As seen in Figure 7(a), the data points are closely aligned with the 45° reference line, indicating that the residuals conform to a normal distribution. This alignment validates the model structure's appropriateness and the trustworthiness of the corresponding ANOVA findings [60]. The high predictive accuracy of the model is corroborated by the robust linear correlation between the experimental MV 2B removal data and the projected values, as seen in Figure 7(b). The graph of externally studentized residuals against run number (Figure 7(c)) exhibited values between −3.0 and +3.0, indicating that the model demonstrated little deviation, with the discrepancies conforming to a normal distribution. Figure 7(d) illustrates the leverage for MV 2B adsorption experiments. The leverage values below 1 suggest that the fitted model's approximation to the response surface is rather accurate, with no data recording errors, and the scattering reflects the impact of all runs on the fitted model [61].

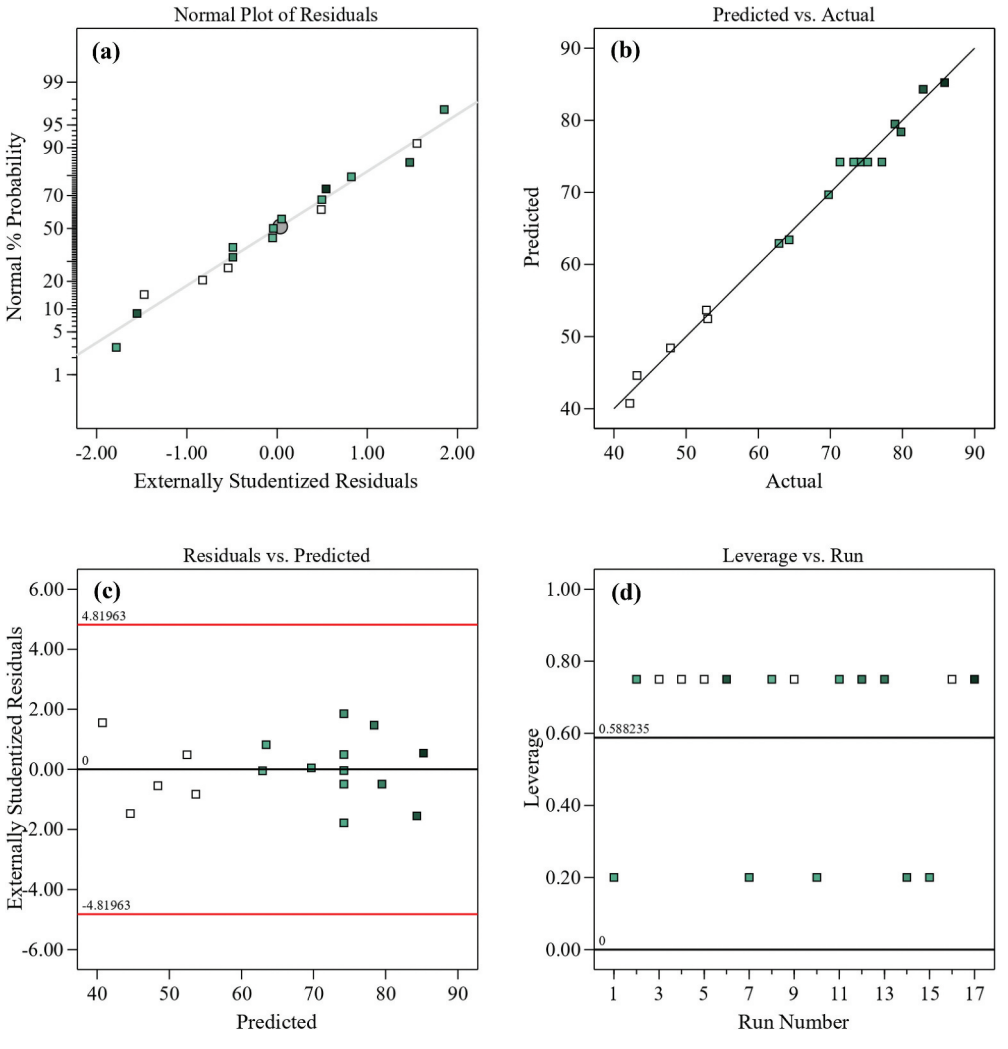

Figure 7. (a) Normal plot of residual AG@CN-PMDA, (b) predicted versus actual, (c) probability plot of externally studentized residuals vs. predicted values, (d) the leverage for the MV 2B adsorption runs.

3.3. Response surface plots

A comprehensive analysis was conducted to thoroughly understand the relationships between independent variables and the effectiveness of MV 2B removal. This investigation included the development of 3D response surfaces and 2D contours using the quadratic model. All possible combinations of input parameters were meticulously analysed, as seen in Table 3. The substantial impact of AG@CN-PMDA dosage (A) and pH (C) on MV 2B dye removal is shown by the statistically significant p-value of 0.0356 in Table 3. The outcome indicates that the percentage of MV 2B dye removal rose with both the dose of AG@CN-PMDA (A) and the pH level (C), as seen in Figure 8(a,b). The removal rate of MV 2B increases when pH rises from 4 to 10. The analysis in Figure 6 indicates that the pH_{pzc} value of AG@CN-PMDA was determined to be 6.4. In turn, the

surface of AG@CN-PMDA is protonated at pH levels below 6.4 and acquires a negative charge at pH levels above the pH_{pzc}. Thus, at elevated pH values, the acidic groups of AG@CN-PMDA and MV $2B^{+}$ cation are drawn together by electrostatic attraction, as summarized in Equation (5):

$$AG@CN - PMDA^{-} + MV\ 2B^{+} \leftrightarrow AG@CN - PMDA^{-}\ldots{}^{+}MV\ 2B \tag{5}$$

Observations in Figure 8(a,b) suggest that augmenting the dose of AG@CN-PMDA from 0.02 to 0.1 g/100 mL leads to an increase in the adsorption. Increased dosages of AG@CN-PMDA enhance the formation of a greater surface area and more adsorption spots, resulting in superior adsorption efficacy [62]. Figure 8(a,b) shows the 3D and 2D representations of the synergistic effects of time (B) and pH (C) on the removal rate of MV 2B (p-value = 0.0069). The findings indicate that the contact time positively influences the removal rate of MV 2B, showing enhancement as the period extends from 2 to 20 min. This is due to the time necessary for the MV 2B dye to permeate the pores of AG@CN-PMDA, which enhance the adsorption efficacy.

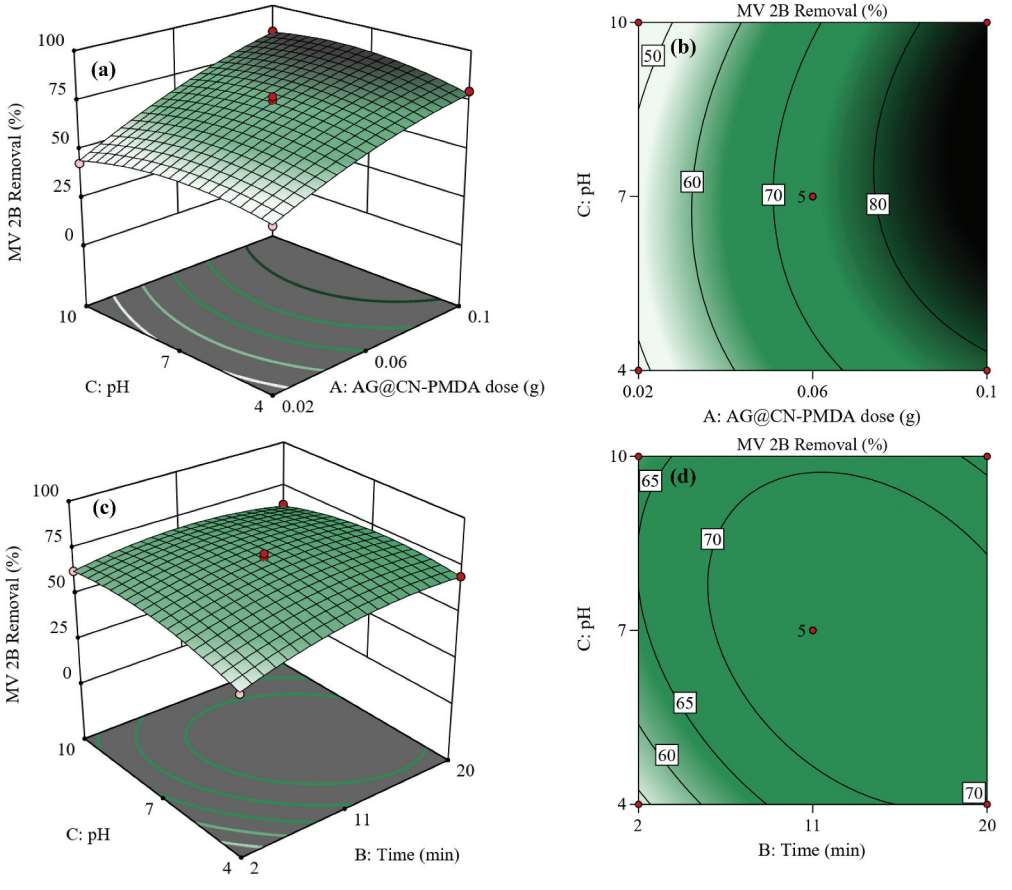

Figure 8. 3D response surfaces and 2D contour plots of AC (a: 3D; b: 2D), and BC (c: 3D; d: 2D).

3.4. Adsorption study

To gain insight into the adsorption properties of AG@CN-PMDA and how it interacts with MV 2B dye, it is crucial to assess the impact of the initial dye concentration on the uptake efficacy of the adsorbent. The adsorption capacity of AG@CN-PMDA was seen to fluctuate based on the initial MV 2B concentration, as depicted in Figure 9(a). In this assessment, the pH of the 250 mL MV 2B solution was adjusted to 6.9 by utilising 0.09 g of AG@CN-PMDA, according to the optimal parameters established by the desirability function. Increasing the starting MV 2B concentration (20–150 mg/L) enhanced the dye adsorption efficiency of AG@CN-PMDA from 14.3 to 120.3 mg/g. This effect may result from an augmentation in the mass transfer driving force, occurring when the dye's initial concentration is raised [63]. The greater driving force causes an increase in the amount of dye that may diffuse into the internal pores of AG@CN-PMDA in the liquid phase.

3.5. Adsorption kinetics

An examination of the adsorption kinetics provides critical understanding of the mechanisms regulating the interaction between AG@CN-PMDA and MV 2B dye. The adsorption behaviour was assessed using two kinetic models: the pseudo-first order (PFO) [64] and pseudo-second order (PSO) [65] equations. The nonlinear equations for these models are outlined in Table S1, and the associated kinetic parameters are detailed in Table 4. The findings of the model fits indicate that the PSO model had superior R^2 values relative to the PFO model. The estimated adsorption capacities derived from the PSO model closely aligned with the experimental values ($q_{e\ exp}$). The trend in the results indicate that chemisorption is the primary mechanism controlling MV 2B adsorption onto the AG@CN-PMDA surface, as corroborated by the kinetic data [66]. The decreased k_2 values obtained at elevated initial levels of MV 2B suggest that the adsorption process needs an extended duration to achieve equilibrium [67]. This behaviour results from the increased concentration of MV 2B dye molecules that competes for the accessible adsorption sites on the AG@CN-PMDA adsorbent.

3.6. Adsorption isotherm

The adsorption isotherms provide an assessment of empirical adsorption data, which provides insight on the adsorption mechanism and the possible interaction between the adsorbate (MV 2B dye) and the adsorbent AG@CN-PMDA. Table 5 displays the characteristics of the adsorption isotherms derived from the utilisation of several models (Langmuir [68], Freundlich [69], and Temkin [70]). Descriptions of the nonlinear forms of Langmuir, Freundlich, and Temkin are presented in Table S1. Figure 9 (a) displays the fitted curves for the adsorption isotherms, and the values for the isotherms that were evaluated are listed in Table 5. The Temkin isotherm exhibited the most favourable match to the experimental data ($R^2 = 0.99$) underscoring the critical influence of adsorbate-adsorbent interactions and the energy fluctuations over the adsorption surface. The adsorption heat ($b_T = 36.3$ J/mol) suggests that the potential for both physisorption and chemisorption contributions. such as the equilibrium binding constant ($K_T = 1.21$ L/mg) is situated within the range of 1 to 10,

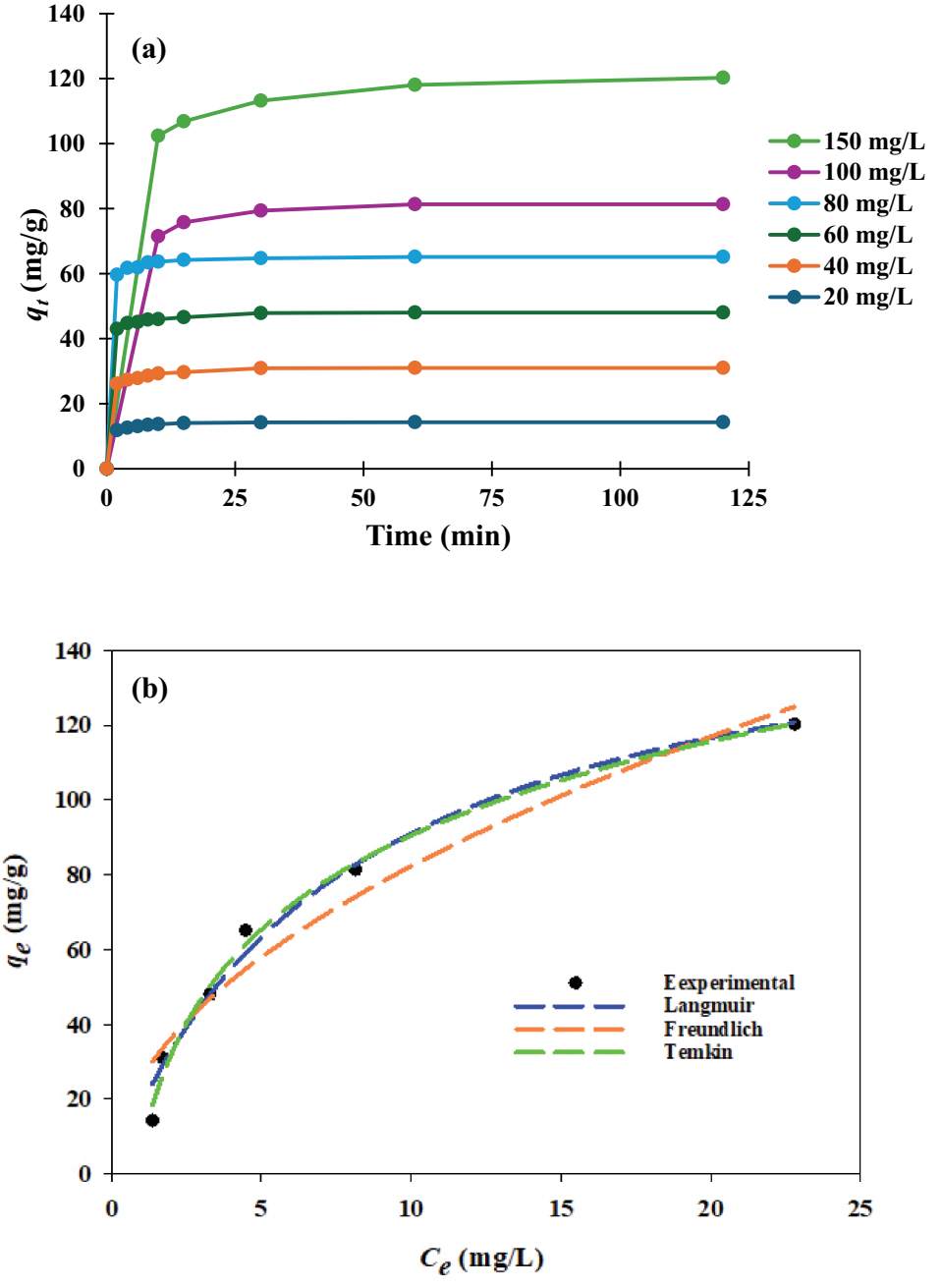

Figure 9. (a) Effect of initial MV 2B dye concentration on the adsorption ability of AG@CN-PMDA; and (b) adsorption isotherms of MV 2B (AG@CN-PMDA dose = 0.09 g/100 mL, solution pH = 6.9, temperature = 25°C, and agitation speed = 100 rpm).

indicating moderate binding strength and a favourable adsorption process [71,72]. Moreover, Langmuir isotherm exhibited a robust correlation ($R^2 = 0.98$), indicating monolayer adsorption with a maximum adsorption capacity ($q_{max} = 162.3$ mg/g),

Table 4. PFO and PSO kinetic parameters for the adsorption of MV 2B by AG@CN-PMDA composite.

		PFO			PSO		
Concentration (mg/L)	$q_{e\ exp.}$(mg/g)	$q_{e\ cal}$ (mg/g)	k_1 (1/min)	R^2	$q_{e\ cal}$ (mg/g)	k_2 x 10^{-2} (g/mg min)	R^2
20	15.9	13.8	0.89	0.63	14.3	0.1464	0.96
40	33.1	29.6	0.99	0.98	28.3	0.0898	0.99
60	51.1	46.6	1.24	0.99	47.7	0.0848	0.99
80	71.3	63.8	1.33	0.98	64.1	0.0784	0.99
100	91.5	80.5	0.21	0.97	93.1	0.0077	0.99
150	144.9	116.8	0.19	0.99	141.7	0.0042	0.99

Table 5. The parameters of the adsorption isotherm models and equilibrium parametersfor MV 2B by AG@CN-PMDA composite.

Adsorption isotherm	Parameter	Value
Langmuir	q_{max} (mg/g)	162.3
	K_a (L/mg)	0.13
	R^2	0.98
Freundlich	K_f (mg/g) (L/mg)$^{1/n}$	25.7
	n	1.97
	R^2	0.94
Temkin	K_T (L/mg)	1.21
	b_T (J/mol)	68.3
	R^2	0.99

reflecting high affinity between the AG@CN-PMDA surface with MV 2B. The Freundlich isotherm ($R^2 = 0.94$) indicated the existence of heterogeneous adsorption sites, with a value of $n = 1.97$, implying favourable adsorption. This indicates a strong affinity between the adsorbent and the adsorbate, since (n) values ranging from 1 to 10 are often regarded as favourable adsorption processes.

Table 6 presents a comparative analysis of the q_{max} values obtained in this study with those of other adsorbents reported for MV 2B removal. The results demonstrate that AG@CN-PMDA exhibits a superior adsorption capacity, confirming its efficiency and potential as an excellent adsorbent for dye-contaminated wastewater.

3.7. Dye adsorption thermodynamics

The thermodynamic analysis, encompassing variations in Gibbs free energy ($\Delta G°$), enthalpy ($\Delta H°$), and entropy ($\Delta S°$), was conducted to gain further insight into the

Table 6. Comparison of the adsorption capacity of AG@CN-PMDA towards MV 2B with different adsorbents.

Adsorbents	q_{max} (mg/g)	References
AG@CN-PMDA	162.3	This study
Iraqi date seeds	59.5	[73]
Magnetic kaolin/TiO_2/γ-Fe_2O_3 nanocomposite	131.58	[74]
Natural Moroccan Zeolite	30.3	[75]
Halloysite-magnetite composite	90.91	[76]
NaOH-treated *Cucumis melo var. cantalupensis* (rock melon) skin	224.56	[77]
Stem axis of *Artocarpus odoratissimus* fruit (TSA)	263.7	[78]
Ipomoea aquatica (Aquatic plant)	267.9	[79]

adsorption behaviour of MV 2B onto the AG@CN-PMDA composite [80]. This evaluation aimed to identify whether the adsorption process is predominantly driven by enthalpic or entropic contributions. The thermodynamic parameters $\Delta G°$, $\Delta H°$, and $\Delta S°$, along with the equilibrium constant (K), were calculated using Equations (6)–(8).

$$\Delta G^{\circ} = -RT\ln K_d \tag{6}$$

$$K_d = \frac{q_e}{C_e} \tag{7}$$

$$\ln K_d = \frac{\Delta S^{\circ}}{R} - \frac{\Delta H^{\circ}}{RT} \tag{8}$$

The thermodynamic parameters for enthalpy ($\Delta H°$) and entropy ($\Delta S°$) were determined from the slope and intercept of the linear van't Hoff plot ($\ln K_d$ vs. 1/T) as illustrated in Figure 10. A summary of the calculated values for $\Delta G°$, $\Delta H°$, and $\Delta S°$ are provided in Table 7. The negative values of $\Delta G°$ across all tested temperatures confirm the spontaneous nature of MV 2B adsorption onto the AG@CN-PMDA surface [81]. Furthermore, the positive enthalpy change ($\Delta H° = 15.7$ kJ/mol) indicates that the adsorption process is endothermic and entropy-driven in nature, where chemisorption likely plays a dominant role in the interaction mechanism [82]. Furthermore, the positive entropy value ($\Delta S° = 0.07$ J/mol K) suggests that the adsorbent-adsorbate interface becomes more random during the adsorption process, which is attributed to desolvation effects [83]. The results indicate that the adsorption of MV 2B is more advantageous at elevated temperatures, aligning with the endothermic adsorption process. The results of the thermodynamic functions supported the Temkin isotherm model, and reinforce the conclusion that the potential for both physisorption and chemisorption contributions under the examined adsorption conditions.

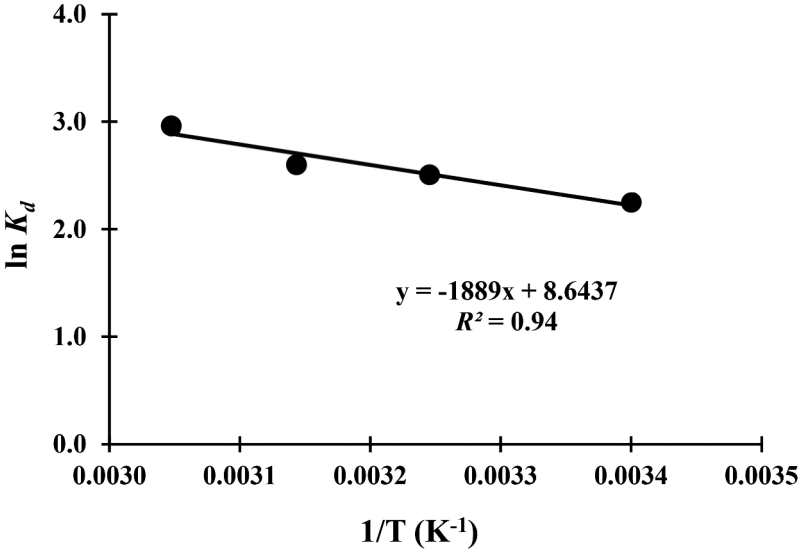

Figure 10. van't Hoff plot for the adsorption of MV 2B onto AG@CN-PMDA adsorbent. The following conditions apply: dose = 0.09 g/100 mL, pH = 6.9, agitation speed = 100 rpm.

Table 7. Thermodynamic adsorption parameters for MV 2B with the AG@CN-PMDA composite.

T (K)	K_d	$\Delta G°$ (kJ/mol)	$\Delta H°$ (kJ/mol)	$\Delta S°$ (J/mol K)
298.15	9.5	−5.72	15.7	0.07
308.15	12.3	−6.44		
318.15	13.5	−7.16		
328.15	19.3	−7.88		

3.8. Adsorption mechanism

The adsorption of MV 2B dye is influenced by a complex interaction of elements, including the functional groups on the AG@CN-PMDA, the dye's intrinsic chemical properties, and the ambient conditions during adsorption. The adsorption mechanism of MV 2B dye onto AG@CN-PMDA encompasses electrostatic attractions, π-π stacking, *n*-π interactions, and hydrogen bonding. The positively charged imine groups of MV 2B engage in electrostatic interactions with negatively charged functional groups on AG@CN-PMDA, including carboxylate (-COO^-) and deprotonated hydroxyl (-O^-) groups [25]. π-π stacking occurs between the aromatic rings of MV 2B and the aromatic systems introduced by PMDA functionalization in AG@CN-PMDA, whereas *n*-π interactions engage the lone pairs of nitrogen atoms in MV 2B with the π-systems of PMDA, as well as the lone pairs on nitrogen (from -NH_2) or oxygen (from -OH/-COO^-) in the material and the aromatic rings of MV 2B [84]. In addition, hydrogen bonding occurs between the nitrogen atoms in MV 2B and the hydroxyl (–OH) and amine (-NH_2) groups on AG@CN-PMDA [85] as depicted in Figure 11. This stable and high-capacity adsorption process is the result of the synergistic

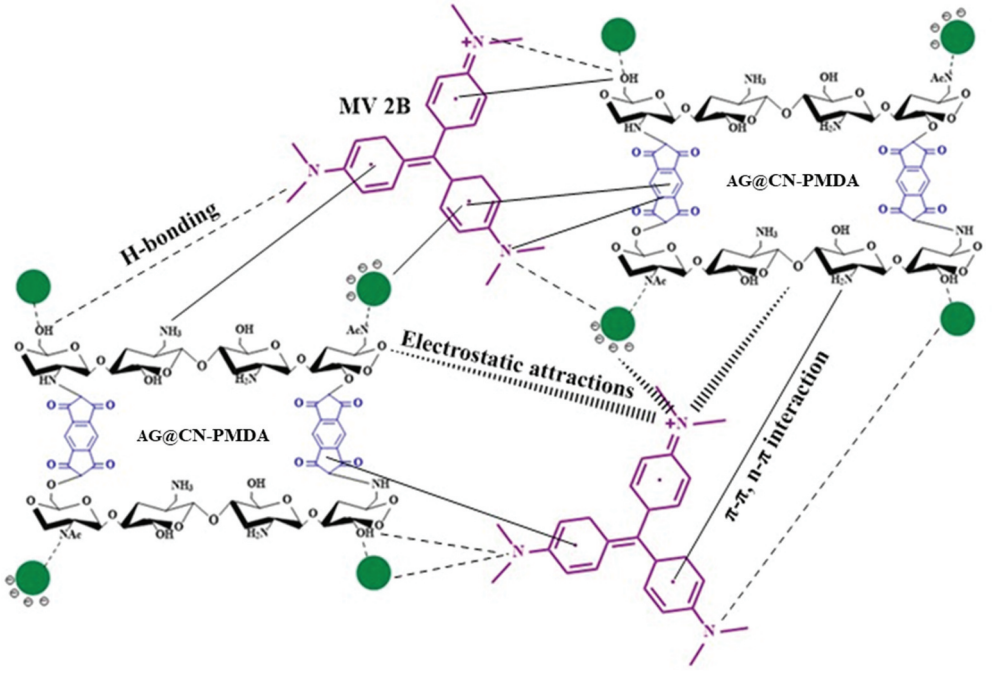

Figure 11. Illustration of the possible interaction between the AG@CN-PMDA adsorbent and the MV 2B dye system, which includes electrostatic attractions, hydrogen bonding, *n*–π, and π–π interactions.

interactions between the material's functional groups and the dye's aromatic and cationic nature, which ensure efficient adsorption.

4. Conclusion

This study demonstrates the successful synthesis of the AG@CN-PMDA composite via the integration of AG biomass into a CN matrix, followed by structural reinforcement via cross-linking with PMDA using a hydrothermal method. The AG@CN-PMDA composite exhibited high efficiency in the removal of MV 2B cationic dye from aqueous media. Optimisation via RSM-BBD revealed a maximum removal of 86% under optimal conditions: adsorbent dose of 0.09 g/100 mL, pH 6.9, and contact time of 9.45 min. Isotherm analysis indicated that the adsorption process conformed well to both the Temkin ($R^2 = 0.99$) and Langmuir ($R^2 = 0.98$) models. The Temkin fit suggests significant adsorbate – adsorbent interactions and the influence of adsorption energy, while the Langmuir model supports the formation of a monolayer with homogeneous adsorption sites, and a maximum adsorption capacity (q_{max}) of 162.3 mg/g. The Freundlich model also showed reasonable correlation ($R^2 = 0.94$), implying some degree of surface heterogeneity and multilayer formation. Kinetic analysis followed a PSO model, confirming that chemisorption is the dominant rate-controlling mechanism, with possible physisorption effects at higher dye concentrations. Thermodynamic evaluation revealed a spontaneous and endothermic process, characterised by a positive enthalpy change ($\Delta H° = 15.7$ kJ/mol) and a positive entropy change ($\Delta S° = 0.07$ J/mol· K), indicating an entropy-driven process. Overall, the AG@CN-PMDA composite exhibits promising potential as an efficient adsorbent for the treatment of cationic dye-contaminated wastewater.

Acknowledgments

The authors would like to thank the Faculty of Applied Sciences, Universiti Teknologi MARA (UiTM) for research facilities. The author (Zeid A. ALOthman) is thankful to the Ongoing Research Funding programme - Research Chairs (ORF-RC-2025-1509), King Saud University, Riyadh, Saudi Arabia.

Disclosure statement

No potential conflict of interest was reported by the author(s).

ORCID

Ali H. Jawad http://orcid.org/0000-0002-4827-9093
Lee D. Wilson http://orcid.org/0000-0002-0688-3102
Hussein A. Kazem http://orcid.org/0000-0002-5034-2485
Zeid A. ALOthman http://orcid.org/0000-0001-9970-2480

Authors contributions

All authors contributed to the study conception and design. Material preparation, data collection and analysis were performed by Hasan M. Agha, Muna Abd Ul Rasool AL-Kazragi, Ali H. Jawad, Lee D. Wilson, Zeid A. ALOthman, and Hussein A. Kazem. The first draft of the manuscript was written by

Hasan M. Agha and all authors commented on previous versions of the manuscript. All authors read and approved of the final manuscript.

Data availability statement

The datasets used and/or analysed during the current study are available from the corresponding author on reasonable request.

References

[1] S.R. Metta and U.K. Sahu, AUIQ Complement Biol. Syst. **2** (1), 77–89 (2025). doi:10.70176/3007-973X.1025
[2] P. Sharma, D. Dutta, A. Udayan and S. Kumar, J. Environ. Chem. Eng. **9** (6), 106673 (2021). doi:10.1016/j.jece.2021.106673
[3] I. Smith, Sci. Insights. **43** (4), 1079–1086 (2023). doi:10.15354/si.23.re801
[4] S. Jan, A.K. Mishra, M.A. Bhat, M.A. Bhat and A.T. Jan, Environ. Sci. Pollut. Res. Int. **30** (53), 113242–113279 (2023). doi:10.1007/s11356-023-30302-4
[5] R.H. Thabet, M.K. Fouad, I.A. Ali, S.A. El Sherbiney and M.A. Tony, Int. J. Environ. Anal. Chem. **103** (11), 2636–2658 (2023). doi:10.1080/03067319.2021.1896716/
[6] N.F. Mohammad Ali, M.A.K. Megat Hanafiah, S.H. Saleh, M.T. Mohd Ali and S. Ibrahim, AUIQ Complement Biol. Syst. **1** (2), 31–45 (2024). doi:10.70176/3007-973X.1013
[7] G.N. Murthy and U.K. Sahu, AUIQ Complement Biol. Syst. **2** (1), 35–48 (2025). doi:10.70176/3007-973X.1024
[8] A. Haleem, A. Shafiq, S.-Q. Chen and M. Nazar, Molecules **28** (3), 1081 (2023). doi:10.3390/molecules28031081
[9] M. Sadiku, T. Selimi, A. Berisha, A. Maloku, V. Mehmeti, V. Thaçi and N. Hasani, Toxics **10** (8), 445 (2022). doi:10.3390/toxics10080445
[10] Y. Kerzabi, A. Benomara and S. Merghache, Glob. Nest J. **24**, 706–719 (2022). doi:10.30955/gnj.004347
[11] R.R. Raja Derisa, H.F. Awang, M. Hakim Azman, I.N.H.A. Rashid, A. Hapiz, R. Wu, A. Reghioua, Z. M. Yaseen and L.D. Wilson, AUIQ Complement Biol. Syst. **2** (1), 60–76 (2025). doi:10.70176/3007-973X.1023
[12] X. Li, T. Tian, T. Cui, B. Liu, R. Jin and J. Zhou, Waste Manag. **170**, 40–49 (2023). doi:10.1016/j.wasman.2023.07.034
[13] M. Malhotra, A. Sudhaik, P. Raizada, T. Ahamad, V.H. Nguyen, Q. Van Le, R. Selvasembian, A. K. Mishra and P. Singh, Ind. Crops Prod. **202**, 117000 (2023). doi:10.1016/j.indcrop.2023.117000
[14] E.A. Hameed, R.A. Salih, A.M. Saleh, H.M. Issa and M.A. Abdulqader, AUIQ Complement Biol. Syst. **1** (1), 52–59 (2024). doi:10.70176/3007-973X.1006
[15] F.N. Türk, H. Çiftçi and H. Arslanoğlu, Sugar Tech. **25** (3), 569–579 (2023). doi:10.1007/s12355-022-01207-2
[16] Q.F. Alsalhy, A.A. Mohammed, S.H. Ahmed, K.T. Rashid and M.A. AlSaadi, Desalin. Water Treat. **108**, 235–245 (2018). doi:10.5004/dwt.2018.21929
[17] K. Saini, A. Sahoo, J. Kumar, A. Kumari, K.K. Pant, A. Bhatnagar and T. Bhaskar, Environ. Res. **231**, 116165 (2023). doi:10.1016/j.envres.2023.116165
[18] M. Sharma, L. Yadav, P. Sharma, V.C. Janu and R. Gupta, Coord. Chem. Rev. **517**, 216008 (2024). doi:10.1016/j.ccr.2024.216008
[19] S. Kumari, J. Chowdhry, M. Kumar and M.C. Garg, Environ. Res. **260**, 119782 (2024). doi:10.1016/j.envres.2024.119782
[20] E.S.A. Haggag, M.A. Embaby, A.S. El-Sheikh, N.A. Fathy and A.A. El-Kady, Int. J. Environ. Anal. Chem. **105** (11), 2552–2568 (2024). doi:10.1080/03067319.2024.2324064

[21] A.H. Almarri, Int. J. Environ. Anal. Chem. **103** (14), 3212–3223 (2023). doi:10.1080/03067319.2021.1896716
[22] P. Bhatt, S. Joshi, G.M.U. Bayram, P. Khati and H. Simsek, Environ. Res. **226**, 115530 (2023). doi:10.1016/j.envres.2023.115530
[23] I. Aranaz, A.R. Alcántara, M.C. Civera, C. Arias, B. Elorza and A. Heras Caballero, N. Acosta, Polym. **13** (19), 3256 (2021). doi:10.3390/polym13193256
[24] C. Pan, J. Qian, C. Zhao, H. Yang, X. Zhao and H. Guo, Carbohydr. Polym. **241**, 116349 (2020). doi:10.1016/j.carbpol.2020.116349
[25] H.M. Agha, A.S. Abdulhameed, R. Wu, A.H. Jawad, Z.A. ALOthman and S. Algburi, Int. J. Phytorem. **26** (8), 1348–1358 (2024). doi:10.1080/15226514.2024.2318777
[26] A. Haider, S. Khan, D.N. Iqbal, S.U. Khan, S. Haider, K. Mohammad, G. Mustfa, M. Rizwan and A. Haider, Int. J. Biol. Macromol. **278**, 134172 (2024). doi:10.1016/j.ijbiomac.2024.134172
[27] K. Zhang, Y. Liu, X. Shi, R. Zhang, Y. He, H. Zhang and W. Wang, Int. J. Biol. Macromol. **242**, 125192 (2023). doi:10.1016/j.ijbiomac.2023.125192
[28] R.M. Visan and D.G. Angelescu, J. Phys. Chem. B. **127** (25), 5718–5729 (2023). doi:10.1021/acs.jpcb.3c02115
[29] W. Lai, L. Wang, Y. Pang, M. Xin, M. Li, L. Shi and Y. Mao, Food Chem. **455**, 139908 (2024). doi:10.1016/j.foodchem.2024.139908
[30] S. Peng, Y. Liu, Z. Xue, W. Yin, X. Liang and M. Li, J. Chang, Cellulose. **24** (11), 4793–4806 (2017). doi:10.1007/s10570-017-1463-y
[31] S. Elhady, M. Bassyouni, M.Z. Elshikhiby, M.Y. Saleh and M.H. Elzahar, Appl Water Sci. **14** (7), 159 (2024). doi:10.1007/s13201-024-02210-6
[32] A. Mahmood, N. Maher, F. Amin, A.Y. Alqutaibi, N. Kumar and M.S. Zafar, Int. J. Biol. Macromol. **268**, 131823 (2024). doi:10.1016/j.ijbiomac.2024.131823
[33] C.D. Pham, T.M. Truong, T.B. Ly and P.K. Le, Waste. Biomass. Valor. **15** (3), 1881–1894 (2024). doi:10.1007/s12649-023-02353-8
[34] H.M. Agha, A.S. Abdulhameed, A.H. Jawad, T. Khadiran, Z.A. ALOthman and L.D. Wilson, J. Inorg. Organomet. Polym. **35** (2), 1084–1099 (2025). doi:10.1007/s10904-024-03327-6
[35] T.U. Rahman, H. Roy, A.Z. Shoronika, A. Fariha, M. Hasan, M.S. Islam, H.M. Marwani, A. Islam, M. M. Hasan, A.K. Alsukaibi and M.M. Rahman, J. Mol. Liq. **388**, 122764 (2023). doi:10.1016/j.molliq.2023.122764
[36] S. Khorshidi, F. Khoobbakht, L. Mirmoghtadaie and S.M. Hosseini, Food Hydrocoll. **145**, 109038 (2023). doi:10.1016/j.foodhyd.2023.109038
[37] R. Ahmad Raus, W.M.F. Wan Nawawi and R.R. Nasaruddin, Asian J. Pharm. Sci. **16** (3), 280–306 (2021). doi:10.1016/j.ajps.2020.10.001
[38] S. Das, S. Kumar, A. Kumar Mehta and M.M. Ghangrekar, Bioresour. Technol. **406**, 131038 (2024). doi:10.1016/j.biortech.2024.131038
[39] A. Mojiri, J.L. Zhou, H. Ratnaweera, S. Rezania and M. Nazari, Chemosphere **288**, 132580 (2022). doi:10.1016/j.chemosphere.2021.132580
[40] A.M. Alotaibi, J.S. Alnawmasi, N.A.H. Alshammari, M.A. Abomuti, N.H. Elsayed and M.G. El-Desouky, Int. J. Biol. Macromol. **274**, 133442 (2024). doi:10.1016/j.ijbiomac.2024.133442
[41] A. Abdelfattah, S.S. Ali, H. Ramadan, E.I. El-Aswar, R. Eltawab, S.J. Ho, T. Elsamahy, S. Li, M.M. El-Sheekh, M. Schagerl and M. Kornaros, Environ. Sci. Ecotechnol. **13**, 100205 (2023). doi:10.1016/j.ese.2022.100205
[42] H.M. Agha, A.S. Abdulhameed, A.H. Jawad, S. Aazmi, N.J. Sidik, Y. De Luna, L.D. Wilson, Z. A. ALOthman and S. Algburi, Int. J. Biol. Macromol. **258**, 128792 (2024). doi:10.1016/j.ijbiomac.2023.128792
[43] A.M. Saleh, H.H. Mahdi, A.B. Alias, O.M. Ali, W.A.W.A.K. Ghani, T.A. Shihab, S.S.A.S. Hasan, O. K. Ahmed and N.M. Saleh, Ann. Chim. Sci. Mater. **48** (4), 509 (2024). doi:10.18280/acsm.480408
[44] Y.W. Chen, H.V. Lee, J.C. Juan and S.-M. Phang, Carbohydr. Polym. **151**, 1210–1219 (2016). doi:10.1016/j.carbpol.2016.06.083
[45] H. Yin, B. Wang, M. Zhang and F. Zhang, Int. J. Biol. Macromol. **277**, 134062 (2024). doi:10.1016/j.ijbiomac.2024.134062

[46] Y.W. Yap, N. Mahmed, M.N. Norizan, S.Z. Abd Rahim, M.N. Ahmad Salimi, K. Abdul Razak, I. S. Mohamad, M.M.A.B. Abdullah and M.Y. Mohamad Yunus, Materials **16** (9), 3601 (2023). doi:10.3390/ma16093601
[47] C. Zhang, M. Vehkamäki, M. Pietikäinen, M. Leskelä and M. Ritala, Chem. Mater. **32** (12), 5073–5083 (2020). doi:10.1021/acs.chemmater.0c00898
[48] R.M. Eltabey, F.T. Abdelwahed, M.M. Eldefrawy and M.M. Elnagar, J. Hazard. Mater. **439**, 129589 (2022). doi:10.1016/j.jhazmat.2022.129589
[49] M. Pishnamazi, S.M. Dhiaa, R. Emadi, S.A. Shahrtash, M.R. Jamali, J. Kaur and A. Soltani, J. Mol. Struct. **1303**, 137524 (2024). doi:10.1016/j.molstruc.2024.137524
[50] N.R. Kildeeva, P.A. Perminov, L.V. Vladimirov, V.V. Novikov and S.N. Mikhailov, Russ. J. Bioorg. Chem. **35** (3), 360–369 (2009). doi:10.1134/S106816200903011X
[51] K. Wegrzynowska-Drzymalska, P. Grebicka, D.T. Mlynarczyk, D. Chelminiak-Dudkiewicz, H. Kaczmarek, T. Goslinski and M. Ziegler-Borowska, Materials **13** (15), 3413 (2020). doi:10.3390/ma13153413
[52] H. Toiserkani, Compos. Interface. **30** (2), 187–199 (2023). doi:10.1080/09276440.2022.2084904
[53] U. Jančič, M. Božič, S. Hribernik, T. Mohan, R. Kargl, K.S. Kleinschek and S. Gorgieva, Cellulose **28** (16), 10457–10475 (2021). doi:10.1007/s10570-021-04195-w
[54] N. Gewili, A.M. Abdelghany, M. Mekhaimer and A. Oraby, Lett. Appl. Nanobiosci. **10** (4), 2742–2749 (2021). doi:10.33263/LIANBS104.27422749
[55] Y. Yang, G. Chen, P. Murray and H. Zhang, SN Appl Sci. **2** (3), 435 (2020). doi:10.1007/s42452-020-2252-z
[56] N.R. Palapa, N. Ahmad, A. Wijaya and Z.A. Zahara, Sci. Technol. Indones. **8** (2), 305–311 (2023). doi:10.26554/sti.2023.8.2.305-311
[57] X. Wang, B. Cheng, L. Zhang, J. Yu and Y. Li, J. Colloid. Interface Sci. **612**, 598–607 (2022). doi:10.1016/j.jcis.2021.12.176
[58] D. Bisht, S. Sinha, S. Nigam, K. Bisaria, T. Mehrotra and R. Singh, Water. Sci. Technol. **83** (7), 1662–1676 (2021). doi:10.2166/wst.2021.066
[59] O.A. Awadalla, W.A. Atawy, M.Y. Bedaiwy, S.S. Ali and Y.A.G. Mahmoud, Ind. Crops Prod. **195**, 116420 (2023). doi:10.1016/j.indcrop.2023.116420
[60] Z. Khoshraftar and A. Ghaemi, Curr. Res. Green Sustain. Chem. **5**, 100342 (2022). doi:10.1016/j.crgsc.2022.100342
[61] M. Feilizadeh, M. Rahimi, S.M.E. Zakeri, N. Mahinpey, M. Vossoughi and M. Qanbarzadeh, Can J Chem. Eng. **95** (7), 1228–1235 (2017). doi:10.1002/cjce.22808
[62] L. Leng, Q. Xiong, L. Yang, H. Li, Y. Zhou, W. Zhang, S. Jiang, H. Li and H. Huang, Sci. Total Environ. **763**, 144204 (2021). doi:10.1016/j.scitotenv.2020.144204
[63] E. Rápó and S. Tonk, Molecules **26** (17), 5419 (2021). doi:10.3390/molecules26175419
[64] S. Lagergren and K. Sven, Vetenskapsakad. Handl. **24**, 1–39 (1898). doi:10.1007/BF01501332
[65] Y.S. Ho and G. McKay, Chem. Eng J. **70** (2), 115–124 (1998). doi:10.1016/S0923-0467(98)00076-1
[66] M. Thabet, E.M. Abd El-Monaem, W.R. Alharbi, M. Mohamoud, A.H. Abdel-Aty, I. Ibrahim, M. A. Abdel-Lateef, A.E. Goda, T.A.S. Elnasr, R. Wang and H. Gomaa, J. Water Process Eng. **60**, 105192 (2024). doi:10.1016/j.jwpe.2024.105192
[67] A. Mohammadpour, A. Kazemi, M.A. Baghapour, M.R. Samaei, K. Kannan and A.M. Khaneghah, Int. J. Biol. Macromol. **277**, 134060 (2024). doi:10.1016/j.ijbiomac.2024.134060
[68] I. Langmuir, J. Am. Chem. Soc. **40** (9), 1361–1403 (1918). doi:10.1021/ja02242a004
[69] H.M.F. Freundlich, J. Phys. Chem. **57**, 385–471 (1906).
[70] M.I. Temkin, Acta Physiochim. URSS. **12**, 327–356 (1940). doi:10.1007/978-3-642-79197-0_4
[71] J.S. Piccin, T.R.S. Cadaval, L.A.A. De Pinto and G.L. Dotto, in *Adsorption Processes for Water Treatment and Purification*, edited by A. Bonilla-Petriciolet, D. Mendoza-Castillo, and H. Reynel-Ávila (Springer, Cham, 2017), pp. 19–51. doi:10.1007/978-3-319-58136-1_2
[72] M. Kanagalakshmi, S.G. Devi, P. Ananthi and A. Pius, in *Carbon Nanomaterials and Their Composites as Adsorbents. Carbon Nanostructures*, edited by J. Tharini, and S. Thomas (Springer, Cham, 2024). doi:10.1007/978-3-031-48719-4_8

[73] N.S. Ali, N.M. Jabbar, S.M. Alardhi, H.S. Majdi and T.M. Albayati, Heliyon **8** (8), e10276 (2022). doi:10.1016/j.heliyon.2022.e10276
[74] S. Fındık, Water. Air, Soil Pollut. **235** (8), 514 (2024). doi:10.1007/s11270-024-07334-8
[75] M. El Rharib, K. Hamidallah, Z. Zaroual, S. Elghachtouli and M. Azzi, Environ. Sci. Pollut. Res. **31** (53), 62131–62146 (2024). doi:10.1007/s11356-023-28307-0
[76] L.R. Bonetto, F. Ferrarini, C. De Marco, J.S. Crespo, R. Guégan and M. Giovanela, J. Water Process Eng. **6**, 11–20 (2015). doi:10.1016/j.jwpe.2015.02.006
[77] L.B.L. Lim, N. Priyantha, X.H. Bong and N.A.H.M. Zaidi, Desalin. Water Treat. **180**, 336–348 (2020). doi:10.5004/dwt.2020.24871
[78] M.R.R. Kooh, M.K. Dahri and L.B.L. Lim, Appl. Water Sci. **7** (7), 3573–3581 (2017). doi:10.1007/s13201-016-0496-y
[79] T.L. Kua, M.R.R. Kooh, M.K. Dahri, N.A.H.M. Zaidi, Y. Lu and L.B.L. Lim, Appl. Water Sci. **10** (12), 243 (2020). doi:10.1007/s13201-020-01326-9
[80] H.M. Agha, A.H. Jawad, L.D. Wilson, K. Al-Essa and Z.A. ALOthman, Int. J. Biol. Macromol. **309**, 142752 (2025). doi:10.1016/j.ijbiomac.2025.142752
[81] H.M. Agha, A.H. Jawad, L.D. Wilson and Z.A. ALOthman, Int. J. Environ. Anal. Chem. 1–23 (2024). doi:10.1080/03067319.2024.2426730
[82] G.G. Hacıosmanoğlu, M. Arenas, C. Mejías, J. Martín, J.L. Santos, I. Aparicio and E. Alonso, Int. J. Environ. Res. Public. Health. **20** (3), 2646 (2023). doi:10.3390/ijerph20032646
[83] A.N. Ebelegi, N. Ayawei and D. Wankasi, Open J. Phys. Chem. **10** (3), 166–182 (2020). doi:10.4236/ojpc.2020.103010
[84] S.K. Singh and A. Das, Phys. Chem. Phys. **17** (15), 9596–9612 (2015). doi:10.1039/C4CP05536E
[85] S. Banerjee and B.L. Bhargava, J. Mol. Graph. Model **127**, 108693 (2024). doi:10.1016/j.jmgm.2023.108693